Korean Journal of Remote Sensing, Vol.24, No.1, 2008, pp.79~89

Adaptive Reconstruction of Harmonic Time Series Using Point-Jacobian Iteration MAP Estimation and Dynamic Compositing: Simulation Study

Sang-Hoon Lee †

Department of Industrial Engineering, Kyungwon University

Abstract : Irregular temporal sampling is a common feature of geophysical and biological time series in remote sensing. This study proposes an on-line system for reconstructing observation image series contaminated by noises resulted from mechanical problems or sensing environmental condition. There is also a high likelihood that during the data acquisition periods the target site corresponding to any given pixel may be covered by fog or cloud, thereby resulting in bad or missing observation.

The surface parameters associated with the land are usually dependent on the climate, and many physical processes that are displayed in the image sensed from the land then exhibit temporal variation with seasonal periodicity. A feedback system proposed in this study reconstructs a sequence of images remotely sensed from the land surface having the physical processes with seasonal periodicity. The harmonic model is used to track seasonal variation through time, and a Gibbs random field (GRF) is used to represent the spatial dependency of digital image processes. The experimental results of this simulation study show the potentiality of the proposed system to reconstruct the image series observed by imperfect sensing technology from the environment which are frequently influenced by bad weather. This study provides fundamental information on the elements of the proposed system for right usage in application.

Key Words : Harmonic Model, Adaptive Reconstruction, Dynamic Compositing, GRF, Bayesian MAP Estimation, Point-Jacobian Iteration.

1. Introduction

Information on the temporal variability of land surface parameters such as temperature, albedo and percentage vegetation cover are of vital importance for regional and global environmental studies. The evolution of technology is radically affecting the quantity and quality of data collected through remote sensing. It is now possible to continuously acquire images at regular time intervals. Satellite remote sensing is one of the best tools available to obtain accurate timely information on the earth's surface. The development of multitemporal techniques in remote sensing has been primarily motivated by the difficulty in discriminating between surface material types based on the spectral signatures at a single point

Received 11 February 2008; Accepted 18 February 2008.

† Corresponding Author: Sang-Hoon Lee (shl@kyungwon.ac.kr)

in time. A typical approach for the analysis of temporal patterns in remote sensing data involves the visual examination of temporal sequence of individual pixels using "temporal profile" plotting (Tucker, *et al.*, 1990; Teng, 1990). Multitemporal features have also been exploited through knowledge-based approaches (Goldberg *et al.*, 1983; Carlotto, 1985). Change-detection of remote sensing has played a fundamental role in monitoring the land surface (Singh, 1989; Fung, 1990; Townsend and Justice, 1995; Carlotto, 1997). The importance of change-detection techniques relies on the possibility of identifying changes on the land by analyzing multitemporal images acquired at different time. Recently, statistical pattern recognition techniques have increasingly interested in using multitemporal information for classification of remotely-sensed imagery (Kahzenie *et al.*, 1990; Jeon and Landgrebe, 1999; Melgani and Serpico, 2003). However, the statistical approaches to the analysis of remotely-sensed images sampled at relatively short intervals remain largely unexplored, and few are designed to preserve abundant and useful information of the sequence of high temporal resolution, which is critical for the parameterization of surface processes.

In the multitemporal analysis of remotely-sensed imagery, there is a high likelihood that during the data acquisition periods the target site corresponding to any given pixel may be covered by fog or cloud, thereby resulting in bad or missing observation. The original distribution of radiated intensity in remote sensing is modified by residual effects resulting from imperfect sensing of the target and atmospheric attenuation. The observations of pixels are then spatially correlated. Lee and Crawford (1991) addressed these problems in the adaptive reconstruction technique to analyze the sequential images observed at regular time intervals. The original uncontaminated intensity is supposed to exhibit temporal variation about the mean intensity only dependent on the target characteristics and be corrupted by a spatial operator and spatially-autocorrelated noise. The original intensity series is reconstructed by "automatic unsupervised learning" using the adaptive linear prediction filter and *maximum a posterior* (MAP) restoration filter. Dynamic compositing approach was suggested to recover bad and missing observations by (Lee, 2002). This reconstruction method incorporates temporal variation in physical properties of targets and anisotropic spatial optical properties into image processing. The adaptive system performs the dynamic compositing by obtaining a composite image as a weighted sum of the observed value and the value predicted according to local temporal trend.

The surface parameters associated with the land are usually dependent on the climate of local region, and many physical processes that are displayed in the image sensed from the land then exhibit temporal variation with seasonal periodicity. Of great importance is the need to incorporate temporal variation of the spectral component according to physical properties of targets and climate changes into image processing techniques. For example, reflectance data from the Advanced Very High Resolution Radiometer (AVHRR) that was deployed on the NOAA-n series of polar orbiting meteorological satellites were obtainable globally on a daily basis and had been shown to have considerable potential for large scale land vegetation studies (Horvath *et al.*, 1982; Townsend and Tucker, 1984). Multispectral reflectance data have been transformed and combined into various vegetation indices to minimize the variability due to external factors (Tarpley *et al.*, 1984). The most commonly used vegetation index is the normalized difference vegetation index (NDVI), and the NDVI versus time profile then reflects the seasonal development history of individual

vegetation. The seasonality of physical processes can be represented with a harmonic model which is characterized by four components: level, frequency, amplitude and phase. The parameterization of the harmonic components for an individual pixel provides physically interpretable values to characterize the seasonal variation of local region corresponding to the pixel.

In this study, a feedback system is proposed to reconstruct a sequence of images remotely sensed from the land surface having the physical processes with seasonal periodicity. The harmonic model is used to track seasonal variation through time, and a Gibbs random field (GRF) is used to represent the spatial dependency of digital image processes. Because simultaneous modeling of temporal and spatial components is extremely complex, the feedback system includes the separate filters of each component, which are independently operated. It is natural to suppose that the harmonic parameters change over time. The temporal component filter employs an exponentially weighted method as in the dynamic compositing (Lee, 2002) to adapt to changes over time. For a realization of spectral intensities, the harmonic parameters are sequentially updated over time using an exponentially weighted least squares criterion. The spatial component filter employs the Point-Jacobian iteration MAP estimation based on the GRF (Lee, 2007) to remove the spatially-correlated noise from the observation and estimate the mean intensity, which is associated with target class parameter, using contextual information. In the reconstruction system, missing observation is replaced by the prediction from the harmonic model and bad observation is recovered by the dynamic compositing of quadratic polynomial function. The proposed system was extensively evaluated with simulation data generated by Monte Carlo method. Sections 2 and 3 describe the adaptive harmonic parameter estimation and Point-Jacobian iteration MAP filters, which are the components of the reconstruction system. Section 4 outlines the proposed reconstruction system including the dynamic compositing filter of quadratic polynomial function. Section 5 contains the experimental results using simulation data. Conclusions are presented in Section 6.

2. Adaptive Harmonic Parameter Estimation Filter

The process of seasonality in local region can be represented with a harmonic model whoes components are assumed to be only due to the local characteristics. The level represents the average of spectral intensity over the whole period that the data are compiled. The periodicity of response is described by the frequency. The amplitude reflects the range and the phase the initiation time of variation in the spectral measurements. Thus, the temporal realization of spectral measurements of each pixel can be expressed as a harmonic model according to the seasonal characteristics of the corresponding local region.

A sample image is considered as a set of n pixels and the intensity process can be represented at time t in the form

$$\begin{aligned} \boldsymbol{Y}_t &= \boldsymbol{X}_t + \boldsymbol{\varepsilon}_t \\ \boldsymbol{X}_t &= \boldsymbol{\mu}_t + \boldsymbol{\delta}_t = \{\alpha_i + \gamma_i \sin(\omega_i t + \theta_i),\ i \in I_n\} \end{aligned} \tag{1}$$

where $I_n = \{1,2,\cdots,n\}$ is a set of pixel indices, $\boldsymbol{Y}_t$ and $\boldsymbol{X}_t$ are the observed and original intensity vectors respectively, $\boldsymbol{\varepsilon}_t$ is the spatially-correlated random noise vector, $\boldsymbol{\mu}_t$ is the mean intensity vector associated with local texture, $\boldsymbol{\delta}_t$ is the deviation vector from the mean intensity. Texture involves the spatial distribution of intensity in a local region. It contains important information about the structural arrangement of surfaces and their relationship to their

neighboring surfaces. In this study, the original intensity is assumed to be spatially distributed with a same mean as its neighbor pixels according to the structure of local texture.

The parameters of the harmonic model are derived from the temporal trajectory of each pixel's intensity. The sinusoid form of Eq. (1) for each pixel individually can be restated without the pixel index as

$$x_t = \eta + \gamma \sin(\omega t + \theta) = \eta + \alpha \cos\omega t + \beta \sin\omega t \quad (2)$$

where

$$\gamma = \sqrt{\alpha^2 + \beta^2}$$

$$\tan\theta = \frac{\alpha}{\beta},$$

and for a sequence of $(m + 1)$ time steps, $\{t = t_0, t_1, \cdots, t_m\}$,

$$X_m = \mathbf{H}_m V \quad (3)$$

where

$$X_m = [x_{t_0}, x_{t_1}, \cdots, x_{t_m}]^T$$

$$\mathbf{H}_m = \begin{pmatrix} 1 & \cos\omega t_0 & \sin\omega t_0 \\ 1 & \cos\omega t_1 & \sin\omega t_1 \\ \vdots & \vdots & \vdots \\ 1 & \cos\omega t_m & \sin\omega t_m \end{pmatrix}$$

$$V = [\eta, \alpha, \beta]^T.$$

If the frequency is known, the least-squares estimate of the unknown harmonic parameter vector V is calculated for a given realization series at a pixel site from the following objective function:

$$\min_V \{(X_m - \mathbf{H}_m V)^T (X_m - \mathbf{H}_m V)\}. \quad (4)$$

By taking the first derivative of Eq. (4) as 0, the least-squares estimate is obtained:

$$\hat{V} = (\mathbf{H}_m^T \mathbf{H}_m)^{-1} \mathbf{H}_m^T X_m = \begin{pmatrix} m & \Sigma_t \cos\omega t \\ \Sigma_t \cos\omega t & \Sigma_t \cos^2\omega t \\ \Sigma_t \sin\omega t & \Sigma_t \cos\omega t \sin\omega t \end{pmatrix}$$

$$\begin{pmatrix} \Sigma_t \sin\omega t \\ \Sigma_t \cos\omega t \sin\omega t \\ \Sigma_t \sin^2\omega t \end{pmatrix}^{-1} \begin{pmatrix} \Sigma_t x_t \\ \Sigma_t x_t \cos\omega t \\ \Sigma_t x_t \sin\omega t \end{pmatrix}. \quad (5)$$

The harmonic parameters can be adaptively estimated by using the exponentially weighted least squares criterion. Given a weight $0 < \lambda_h \leq 1$, the estimates of the harmonic parameters are sequentially updated over time for a realization $\{x_{i,t} \mid t = t_0, t_1, \cdots, t_k\}$ at the ith pixel:

$$\hat{V}_{i,t_k} = \begin{pmatrix} \hat{\eta}_{i,t_k} \\ \hat{\alpha}_{i,t_k} \\ \hat{\beta}_{i,t_k} \end{pmatrix} = \begin{pmatrix} L(t_k) & C(t_k) & S(t_k) \\ C(t_k) & C^2(t_k) & CS(t_k) \\ S(t_k) & CS(t_k) & S^2(t_k) \end{pmatrix}^{-1} \begin{pmatrix} \varphi_{x,i}(t_k) \\ \varphi_{c,i}(t_k) \\ \varphi_{s,i}(t_k) \end{pmatrix}. \quad (6)$$

where

$$L(t_k) = \lambda_h^{(t_k - t_{k-1})} L(t_{k-1}) + 1$$

$$C(t_k) = \lambda_h^{(t_k - t_{k-1})} C(t_{k-1}) + \cos\omega t_k$$

$$S(t_k) = \lambda_h^{(t_k - t_{k-1})} S(t_{k-1}) + \sin\omega t_k$$

$$CS(t_k) = \lambda_h^{(t_k - t_{k-1})} CS(t_{k-1}) + \cos\omega t_k \sin\omega t_k$$

$$C^2(t_k) = \lambda_h^{(t_k - t_{k-1})} C^2(t_{k-1}) + \cos^2\omega t_k$$

$$S^2(t_k) = \lambda_h^{(t_k - t_{k-1})} S^2(t_{k-1}) + \sin^2\omega t_k$$

$$\varphi_{x,i}(t_k) = \lambda_h^{(t_k - t_{k-1})} \varphi_{x,i}(t_{k-1}) + x_{t_k}$$

$$\varphi_{c,i}(t_k) = \lambda_h^{(t_k - t_{k-1})} \varphi_{c,i}(t_{k-1}) + x_{t_k} \cos\omega t_k$$

$$\varphi_{s,i}(t_k) = \lambda_h^{(t_k - t_{k-1})} \varphi_{s,i}(t_{k-1}) + x_{t_k} \sin\omega t_k$$

and the initial values of all the elements at time t_{-1} are zero. The weight λ_h is an exponential forgetting factor that introduces a decaying dependence on past observations, thereby allowing the coefficients to track the temporal varying characteristics of the mean intensity process.

3. Point-Jacobian Iteration Map Filter

Image processes are assumed to combine the random fields associated with intensity and texture respectively. The objective measure for determining the optimal restoration of this "double compound stochastic" image process is based on Bayes' theorem. Given an observed image Y, the Bayesian method is to find the MAP estimate from the mode of the posterior probability distribution of the noise-free vector X, or equivalently, to maximize the log-

likelihood function

$$lPN = \ln P(\boldsymbol{Y}|\boldsymbol{X}) + \ln P(\boldsymbol{X}). \quad (7)$$

It is natural that neighboring pixels with more similar intensity levels have a higher probability of having the same level. Based on this idea, spatial interaction can be quantified for image texture processes based on a distance measure between neighboring pixels. If R_i is the index set of neighbors of the ith pixel, $\boldsymbol{R} = \{R_i \mid i \in I_n\}$ is a "neighborhood system" for I_n. A "clique" of $\{I_n, \boldsymbol{R}\}$, c, is a subset of I_n such that every pair of distinct indices in c represents pixels which are mutual neighbors, and C_p denotes the set of all pair-cliques. A GRF relative to the graph $\{I_n, \boldsymbol{R}\}$ on $\boldsymbol{X} = \{x_i \mid i \in I_n\}$ can be defined by specifying the energy function as a quadratic function of $\boldsymbol{X}$:

$$\begin{aligned} P(\boldsymbol{X}) &= z^{-1} \exp\{-E_p(\boldsymbol{X})\} \\ E_p(\boldsymbol{X}) &= \sum_{i \in I_n} \sum_{(i,j) \in C_p} b_{ij}(x_i - x_j)^2 \end{aligned} \quad (8)$$

where b_{ij} is a nonnegative coefficient vector which represents the "bonding strength" of the ith and the jth pixels. This GRF is used to quantify the spatial interaction probabilistically, that is, to provide a type of prior information on the image texture.

The log-likelihood function of Eq. (7), which uses the GRF of Eq. (8) and the additive Gaussian intensity model, is convex, and the MAP estimate of $\boldsymbol{X}$ is obtained by taking the first derivative of the log-likelihood function:

$$\boldsymbol{X} = (\Sigma^{-1} + \boldsymbol{B})^{-1}\Sigma^{-1}\boldsymbol{Y}. \quad (9)$$

where $\mathbf{B} = \{\beta_{ij}\}$ where

$$\beta_{ij} = \begin{cases} -b_{ij} & \text{for } (i,j) \in C_p \\ \sum_{(i,j) \in C_p} b_{ij} & \text{for } i = j \\ 0 & \text{otherwise} \end{cases}$$

The equation (9) can be solved by the point-Jacobian iteration (Varga, 1962). Decomposing the bonding strength matrix into a matrix with the diagonal elements and a matrix with the non-diagonal elements, the equation (9) is rewritten as

$$\begin{aligned} &\boldsymbol{X} = \boldsymbol{M}_d^{-1}\Sigma^{-1}\boldsymbol{Y} - \boldsymbol{M}_d^{-1}\boldsymbol{B}_s\boldsymbol{X} \\ &\boldsymbol{M}_d = diagonal\{\sigma_k^{-2} + \beta_{kk}, k \in I_n\}. \\ &\boldsymbol{B}_s = \{\beta_{ij} \mid \beta_{ii} = 0\} \end{aligned} \quad (10)$$

The noise-free intensity is recovered iteratively: given an initial estimate of x_i, $\hat{x}_i^0$ at the hth iteration for the ith pixel and a constant r

$$\hat{x}_i^h = \frac{1}{\sigma_i^{-2} + \beta_{ii}} \left[\sigma_i^{-2} y_i - \sum_{(i,j) \in C_p} \beta_{ij} \hat{x}_j^{h-1} \right], \forall_i \in I_n. \quad (11)$$

where $\beta_{ii} = \pi_i$ and $\beta_{ij} = -\pi_i b_{ij}$ for $i \neq j$ where

$$b_{ij} = \begin{cases} \dfrac{(y_i - y_j)^{-2}}{\sum_{(i,j) \in C_p} (y_i - y_k)^{-2}} & \text{for } (i,j) \in C_p \\ 0 & \text{otherwise} \end{cases}$$

$$\pi_i = \sqrt{\frac{r}{\sigma_i^2 \sum_{(i,j) \in C_p} b_{ij}(y_i - y_j)^2}}, \forall_i \in I_n.$$

The iteration converges to a unique solution since $\gamma(\mathbf{M}_d^{-1}\mathbf{B}_s) < 1$ where $\gamma(\bullet)$ denotes the spectral radius (Cullen, 1972). The constant r is a parameter related to the distribution of Y and its appropriate choice is unit value.

The variance σ_i^2 can be estimated using the average value of observed intensities of the ith pixel and its neighbors:

$$\hat{\sigma}_i^2 = \frac{(y_i - \hat{\mu}_i)^2 + \Sigma_{j \in R_i}(y_j - \hat{\mu}_i)^2}{(n_{neighbor} + 1)} \quad (12)$$

where

$$\hat{\mu}_i = \frac{y_i + \Sigma_{j \in R_i} y_j}{(n_{neighbor} + 1)}.$$

The initial estimates $\{\hat{x}_i^0\}$ can be chosen as $\{\hat{\mu}_i\}$ and given a constant for $k_c \ll 1$, a threshold for the condition of convergence in (11) can be defined as

$$\frac{\Sigma_{i \in I_n} |\hat{x}_i^{h-1} - \hat{x}_i^h|}{n} \leq k_c \sqrt{\frac{\Sigma_{i \in I_n} \hat{\sigma}_i^2}{n}} \quad (13)$$

where $k_c \ll 1$ is a given constant.

4. Reconstrunction System WTH Dynamic Compositing

In the reconstruction system, missing observation is replaced by the prediction from the harmonic model and bad observation is recovered by the dynamic compositing of quadratic polynomial function. For a given observation sequence $\{y_{t,i} \mid t = t_0, t_1, \cdots, t_k\}$ for the ith pixel,

$$\begin{aligned} y_{t,i} &= y_{t,i}^{prd} = \hat{\eta}_{t,i} + \hat{\alpha}_{t,i} \cos \omega t + \hat{\beta}_{t,i} \sin \omega t && \text{if } y_{t,i}^{obs} \text{ is missing} \\ y_{t,i} &= y_{t,i}^{cms} = \hat{c}_{0,t,i} + \hat{c}_{1,t,i} t + \hat{c}_{2,t,i} t^2 && \text{if } y_{t,i}^{obs} \text{ is bad.} \\ y_{t,i} &= y_{t,i}^{obs} && \text{otherwise} \end{aligned} \quad (14)$$

In Eq. (14), $\{\hat{c}_{0,t,i}, \hat{c}_{1,t,i}, \hat{c}_{2,t,i}\}$ are the adaptive quadratic polynomial coefficients for the dynamic compositing, which are calculated as

$$\begin{bmatrix} \hat{c}_{0,t_k,i} \\ \hat{c}_{1,t_k,i} \\ \hat{c}_{2,t_k,i} \end{bmatrix} = \begin{bmatrix} \tilde{\phi}_{0,i}(t_k) & \tilde{\phi}_{1,i}(t_k) & \tilde{\phi}_{2,i}(t_k) \\ \tilde{\phi}_{1,i}(t_k) & \tilde{\phi}_{2,i}(t_k) & \tilde{\phi}_{3,i}(t_k) \\ \tilde{\phi}_{2,i}(t_k) & \tilde{\phi}_{3,i}(t_k) & \tilde{\phi}_{4,i}(t_k) \end{bmatrix}^{-1} \begin{bmatrix} \tilde{\varphi}_{0,i}(t_k) \\ \tilde{\varphi}_{1,i}(t_k) \\ \tilde{\varphi}_{2,i}(t_k) \end{bmatrix} \quad (15)$$

where

$$\tilde{\phi}_{h,i}(t_k) = \tilde{\lambda}_{t_k,i} \phi_h(t_{k-1}) + t_k^h$$
$$\tilde{\varphi}_{h,i}(t_k) = \tilde{\lambda}_{t_k,i} \varphi_{h,i}(t_{k-1}) + t_k^h y_{t_k,i}^{obs} .$$

ϕ_h and $\varphi_{h,i}$ in Eq. (15) are sequentially updated over time:

$$\begin{aligned} \phi_{h,i}(t_k) &= \lambda_p \phi_h(t_{k-1}) + t_k^h \\ \varphi_{h,i}(t_k) &= \lambda_p \varphi_{h,i}(t_{k-1}) + t_k^h y_{t_k,i}^{obs} \end{aligned} \quad (16)$$

where $\phi_h(t_{-1}) = \varphi_{h,i}(t_{-1}) = 0$.

Note that $\tilde{\lambda}_{t,i}$ in Eq. (15) is the compositing weight at time t for the ith pixel, while and λ_p in Eq. (16) is the exponential forgetting weight. Under the assumption that the prediction of the harmonic model is an good estimate of the realization, the compositing weight is calculated in this study as a value dependent on the distance between the observation and prediction:

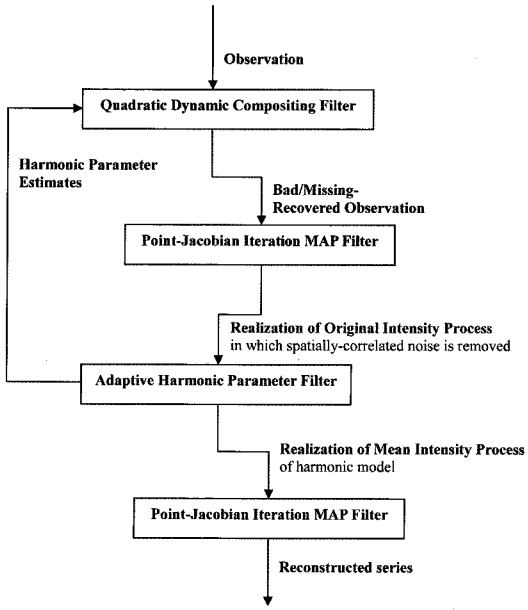

Fig. 1. Outline of reconstruction system.

$$\tilde{\lambda}_{t,i} = 1 - \exp\left(- \sqrt{\frac{(y_{t,i}^{obs} - y_{t,i}^{prd})^2}{\sigma_{i,j}^2}} \right). \quad (17)$$

The proposed reconstruction system outlines in Fig. 1.

5. Experiments

This study assumes that the frequency is known, and all the simulation series were generated for 5 years at two-day time interval and with the frequency of one year. First, the reconstruction system was applied to a simulation harmonic signal which changes its harmonic parameters over time. The observation was simulated by superimposing additive Gaussian noise to the original pattern. The adaptive harmonic parameter estimation filter was evaluated with the simulation signals having the noise of standard deviation of 30. Fig. 2 shows the results including the simulated noisy data. Table 1 contains the values of mean square error which measures the difference between the reconstructed signal and

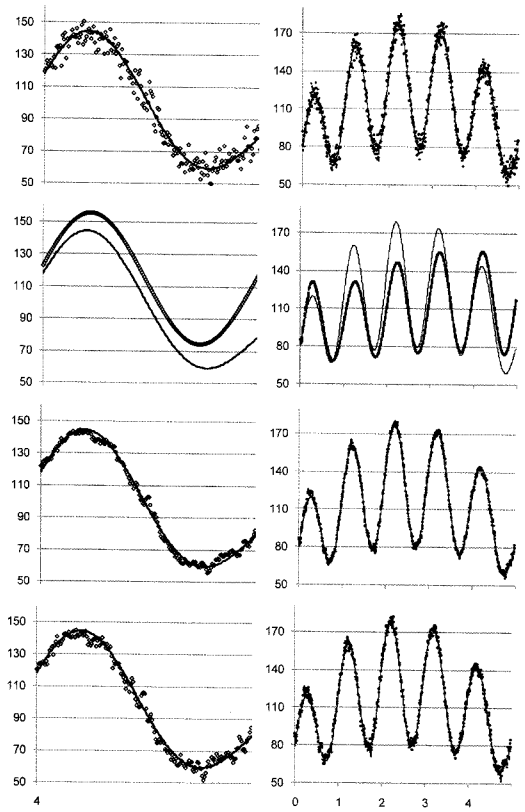

Fig. 2. Reconstructed series with different exponential forgetting weights for observation of noise standard deviation 30: left - for only the 5th year, right - for 5 years (solid line for original pattern).

Table 1. MSE results using various exponential forgetting weights for adaptive harmonic parameter filter

Noise Standard deviation	λ_h	MSE
30	1.0	16.36
	0.9	2.33
	0.8	3.16
	0.7	3.78
70	0.99	8.39
	0.95	5.91
	0.9	6.93
	0.85	7.93

original pattern signal:

$$MSE = \sqrt{\frac{\sum_{\forall t}(\hat{\mu}_t^{rec} - \mu_t^{pat})^2}{n_{timesteps}}}.$$

As shown in these results, the filter fails in tracking the change without the exponentially weighted criterion (that is, $\lambda_h = 1$). The relatively small value of the exponential forgetting weight also results in locally deviating from the original pattern, but not systematically. Fig. 3 shows the estimates of the harmonic parameters over time. It indicates that the small weight makes the estimates too sensitive to the local change of observation. Next the filter was applied to the noisy data with standard deviation of 70, and the results displays in Table 1 and Fig. 4. Comparing to the previous results obtained from the less noisy data, the experiment shows that it is

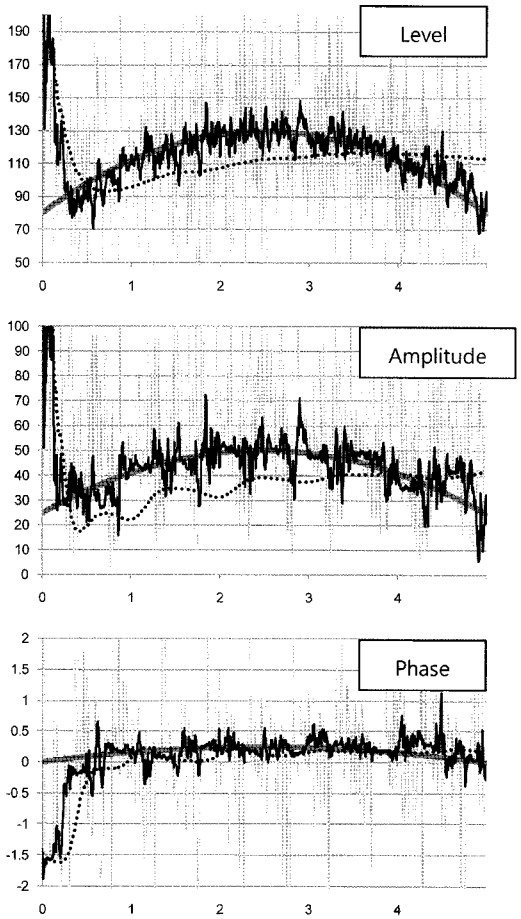

Fig. 3. Estimated harmonic parameters with λ = 1.0 (dot), 0.9 (black solid) and 0.8 (gray solid) respectively: thick and dark gray line for original pattern.

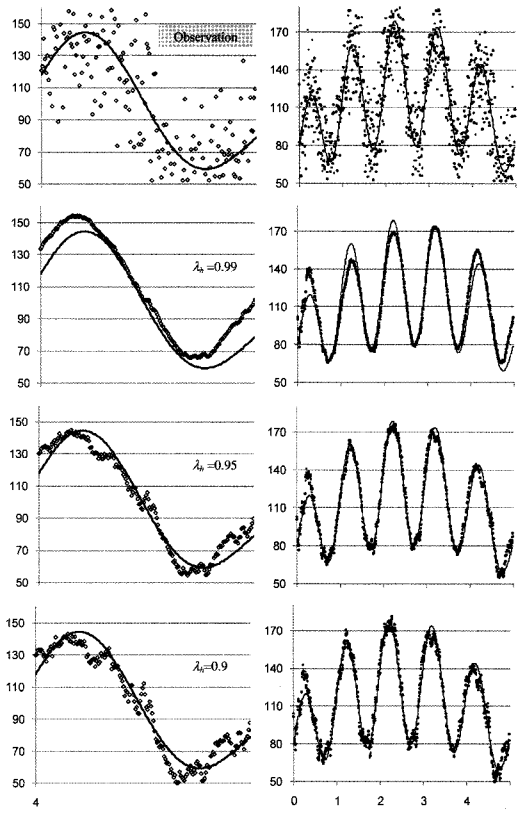

Fig. 4. Reconstructed series with different exponential forgetting weights for observation of noise standard deviation 70: left - for only the 5th year, right - for 5 years (solid line for original pattern).

appropriate to use a larger weight for more noisy data.

The reconstruction system including the dynamic compositing filter was evaluated for the simulation noisy data of standard deviation of 70 generated with missing observation of 35%. Fig. 5 shows the resultant reconstructed series when applying only the dynamic compositing filter, only the adaptive harmonic parameter estimation filter, and both the filters respectively. As.shown in the figure, applying the harmonic filter to the composited series results in yielding more regularized series than to the observation directly. Fig. 6 displays the compositing weights computed over time. Since the exponential forgetting weight, λ_p for the adaptive polynomial

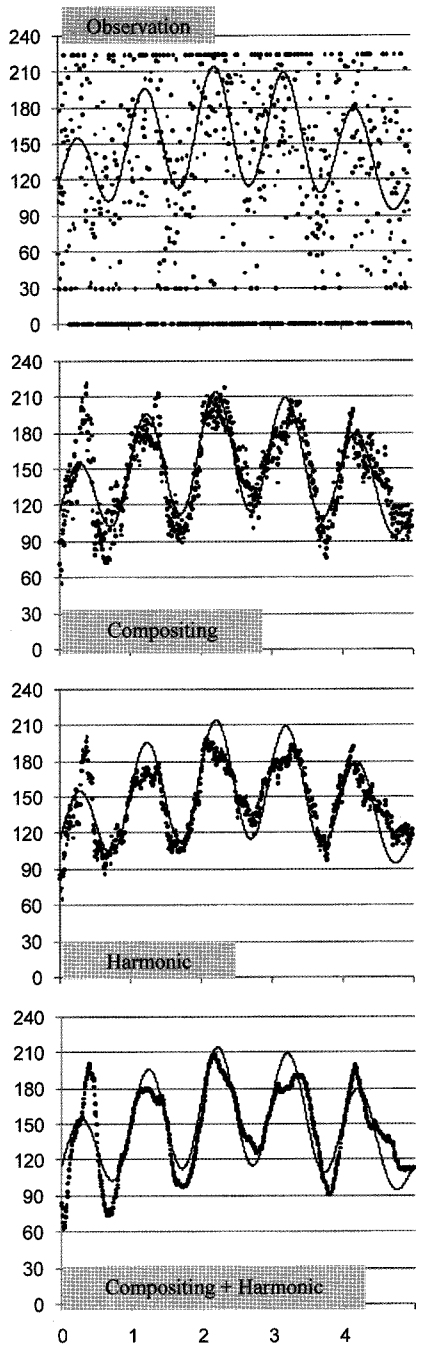

Fig. 5. Reconstructed series with λ_h = 0.97 and λ_p = 0.9 for observation of noise standard deviation 70 and with 35% missing (solid line for original pattern).

coefficient estimation is related to the change of local trend, it is better to use a relatively small weight.

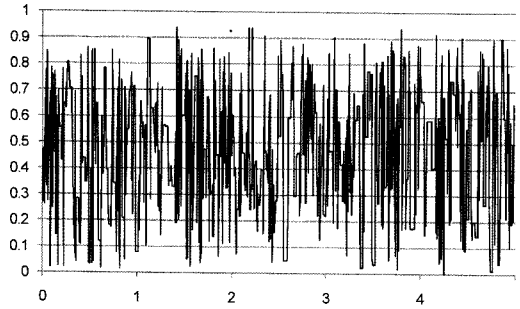

Fig. 6. Compositing weights corresponding to Fig. 5.

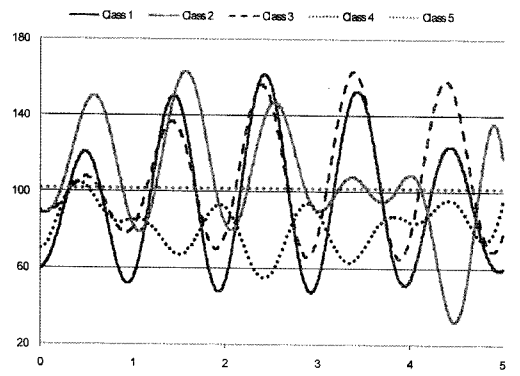

Fig. 7. Mean intensity processes of 5 classes of original pattern.

Last, the whole reconstruction system including the Point-Jacobian MAP filter was applied to the sequence of 912 simulation image generated from the pattern of 5 classes. Each class has different original harmonic patterns which change over time. The missing rates of observation are displayed in Fig. 8. Fig. 9 shows the resultant reconstructed images at 4 time steps of 90-day interval in the 5th year. In this

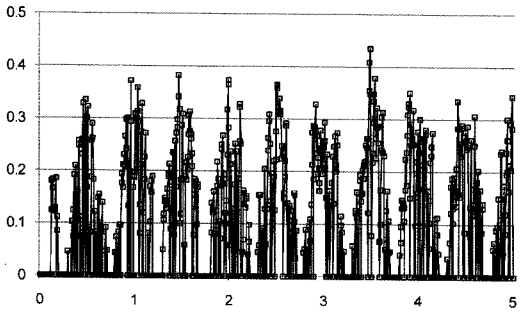

Fig. 8. Missing rates of simulated observation.

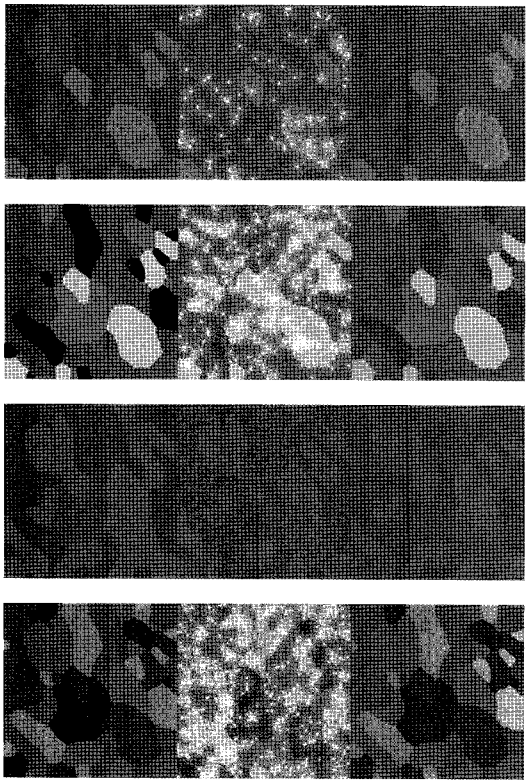

Fig. 9. Reconstructed images at 4 time steps of 90-day interval in the 5th year: mean intensity images of original pattern (left), simulated observation images (center) and reconstructed series images (right).

figure, the bright color in the observation image means missing. The values of *MSE* computed over the image at the individual time step ranges from 3.6 to 27.1.

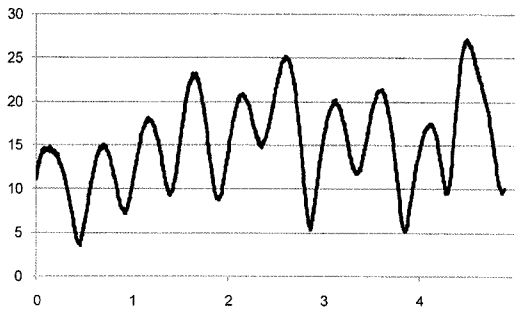

Fig. 10. MSEs of reconstructed image series.

6. Conclusions

This study suggests an adaptive reconstruction system to analyze sequential digital images. The system is effective in recovering the images sensed from the land surface, which generally exhibits temporal variation with seasonal periodicity, and obtaining useful information on seasonal changes from a sequence of contaminated observations. The effectiveness of this reconstruction system is due to combining the temporal and spatial components of physical processes, which are displayed in the observed scene, into image processing. Temporal variation with seasonal periodicity is represented with a harmonic model, and the GRF is used to represent spatial correlation or dependency of neighboring regions in the digital image structure.

The proposed system employs the adaptive scheme using the exponentially weighted least square criterion. The exponential forgetting weights are used to introduce a decaying dependence on past observations, thereby allowing the estimates to track the temporal varying characteristics of the intensity process. It is important to choose an appropriate value between 0 and 1 for the weight to adapt to the changes over time in a right way. The weight very close to 1 may fail in tracking temporal variation at the right time and a relatively small weight may generate a reconstructed series swaying along data fluctuation for a sequence of noisy observations. The quadratic polynomial function is employed to represent a local temporal trend for the dynamic compositing, while the harmonic model represents seasonal characteristics which can be considered as a relatively long-term trend. The forgetting factor of the polynomial model should be chosen as a value smaller than that of the harmonic model, and the weights of smaller values are more ideal for more noisy data.

The experimental results of this simulation study show the potentiality of the proposed system to reconstruct the image series observed by imperfect sensing technology from the environment which are frequently influenced by bad weather. The simple harmonic model with single frequency may not represent the complicated temporal characteristics of the physical processes that have been sensed and displayed in the sequential imagery sufficiently. A general harmonic model with multiple frequencies is more appropriate for temporal processes. The extension to the general model will be the subject of future study.

Acknowledgements

This work was supported in part Korea Research Foundation (Grant #: D00542) and by the Kyungwon University.

References

Carlotto, M. J., 1985. Techniques for multispectral image classification, *SPIE Digital Image Processing*, 528: 174-191.

Carlotto, M. J., 1997. Detection and analysis of change in remotely sensed imagery with application to wide area surveillance, *IEEE Trans. Image Processing*, 6: 189-202.

Cullen, C. G., 1972. *Matrices and Linear Transformations*. Reading, MA: Addison-Wesley.

Fung, T., 1990. An assessment of TM imagery for land-cover change detection, *IEEE Trans. Geosci. Remote Sensing*, 28: 681-684.

Georgii, H. O., 1979. *Canonical Gibbs Measure.*

Berlin, Germany: Springer-Verlag.

Goldberg, M., G. Karem, and M. Alvo, 1983. A production rule-based expert system for interpreting multi-temporal LANDSAT imagery, *CVPR'83 Proceedings.*

Horvath, N. C., T. I. Grey, and D. G. McCray, 1982. Advanced Very High Resolution Radiometer (AVHRR) data evaluation for use in monitoring vegetation, *AgRISTAR Report EW-L@-040303, JSC-18243*, NASA, Lyndon B. Johnson Space Center, Houston, TX., 1982.0-1365.

Jeon, B. and D. A. Landgrebe, 1999. Decision fusion approach for multitemporal classification, *IEEE Trans. Geosci. Remote Sens.*, 37: 1227-1233.

Khazenie, N. and M. M. Crawford, 1990. Spatial-temporal autocorrelated model for contextual classification, *IEEE Trans. Geosci. Remote Sens.*, 28: 529-539.

Lee, S. and M. M. Crawford, 1991. Adaptive reconstruction system for spatially correlated multispectral multitemporal images, *IEEE Trans. on Geosci. Remote Sens.*, 29: 494-503.

Lee, S-H, 2002. Reconstruction and Change Monitoring of Image Series, *Korean Journal of Remote Sensing*, 18: 157-170 (Korean version).

Lee, S-H, 2007. Speckle Removal of SAR Imagery Using a Point-Jacobian Iteration MAP Estimation, *Korean Journal of Remote Sensing*, 23: 33-42.

Melgani, F. and S. B. Serpico, 2003. A Markov random field approach to spatio-temporal contextual image classification, *IEEE Trans. Geosci. Remote Sens.*, 41: 2478-2487.

Tucker, C. J., N. B. Hoblen, J. H. Elgin, Jr, and J. E. Mcmurtey III, 1990. Relationship of spectral data to grain yield variation, *Photogramm. Eng. Remote Sens.*, 46: 657-666.

Teng, W. L., 1990. AVHRR monitoring of US. Crops during the 1988 drought, *Photogramm. Eng. Remote Sens.*, 56: 1143-1146.

Tarpley, J. D., S. R. Schneider, and R. L. Money, 1984. Global vegetation indices from the NOAA-7 meteorological satellite, *J. Climate Appl. Meteorol.*, 23: 491-494.

Singh, A., 1989. Digital change detection techniques using remotely sensed data, *Int. J. Remote Sensing*, 10: 989-1003.

Townsend, J. R. G. and C. J. Tucker, 1984. Objective assessment of AVHRR data for land cover mapping, *Int. J. Remote Sens.*, 5: 492-501.

Townshend, J. R. G. and C. O. Justice, 1995. Spatial variability of imagesand the monitoring of changes in the normalized difference vegetation index, *Int. J. Remote Sensing*, 16(12): 2187-2195.